

# Restoring Connectivity in Vascular Segmentation using a Learned Post-Processing Model

Sophie Carneiro-Esteves<sup>1,2</sup>, Antoine Vacavant<sup>1,2</sup>, and Odysée Merveille<sup>2</sup>

<sup>1</sup> Université Clermont Auvergne, CNRS, SIGMA Clermont, Institut Pascal, F-63000

<sup>2</sup> Univ Lyon, INSA-Lyon, Université Claude Bernard Lyon 1, UJM-Saint Etienne, CNRS, Inserm, CREATIS UMR 5220, U1294,F-69100

**Abstract.** Accurate segmentation of vascular networks is essential for computer-aided tools designed to address cardiovascular diseases. Despite more than thirty years of research, it remains a challenge to obtain vascular segmentation results that preserve the connectivity of the underlying vascular network. Yet connectivity is one of the key feature of these tools. In this work, we propose a post-processing algorithm aiming to reconnect vascular structures that have been disconnected by a segmentation algorithm. Connectivity being a complex property to model explicitly, we propose to learn this geometric feature either through synthetic data or annotations of the application of interest. The resulting post-processing model can be used on the output of any supervised or unsupervised vascular segmentation algorithm. We show that this post-processing effectively restores the connectivity of vascular networks both in 2D and 3D images, leading to improved overall segmentation results.

**Keywords:** Blood vessels, segmentation, connectivity, deep learning, post-processing.

## 1 Introduction

Blood vessel segmentation is a crucial step for various tasks such as blood flow simulation or 3D modeling, and enhancing our understanding of vascular networks physiology, pathologies. However, segmenting blood vessels is challenging due to their thin and tortuous nature, making them easily altered by noise and artefacts. This often results in fragmented blood vessel segmentations which is a major problem for most downstream tasks.

For over thirty years, methods have been introduced to enhance both the quality and the connectivity of blood vessels segmentation. Several unsupervised filtering approaches were first proposed. Vesselness filters [16] aim at enhancing the signal from blood vessels and decrease the one from other non-tubular structures. These filters are designed to detect blood vessels at different scales, employing either a Gaussian-scale paradigm and Hessian-based features extraction [8, 30], or a mathematical morphology approach using paths as structuring elements [21]. These filters are usually the first step of more complex segmentation pipelines [5, 20, 22].

However, determining hyperparameters for these filters can be challenging and there is no guarantee on the connectivity of the vascular tree. Alternative unsupervised methods, such as tracking [3] or minimal path methods [18] can ensure the structure connectivity. Nevertheless, these methods require a time-consuming user interaction to define seed points. All these approaches are further limited by having to explicitly model blood vessels.

Supervised methods, and in particular deep learning-based ones, offer the power to represent complex phenomena by learning implicit functions, provided there are sufficient annotations on the

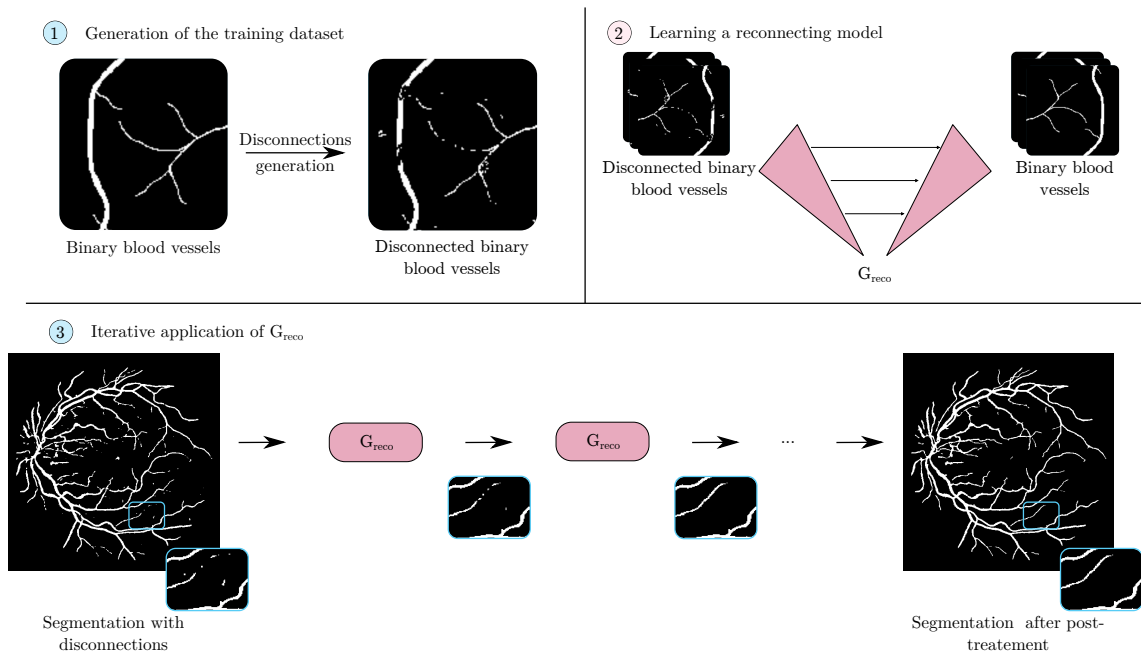


Fig. 1: Pipeline of our method. (1) a dataset is generated containing pairs of connected and disconnected vascular structures. (2) this dataset is used to train a model  $G_{reco}$  with a residual U-Net architecture. (3) finally, the trained model is iteratively applied on a vascular segmentations with disconnections.

target application. Several approaches dedicated to vascular segmentation were proposed [24, 29, 34]. More recently, approaches were developed to improve vascular connectivity of the segmentation results. Classic vesselness filters were used to help the network model tubular shapes [25, 31]. Alternative approaches focused on adapting the segmentation architecture to facilitate the learning of a function that preserves connectivity. Attention modules [36] were incorporated into architectures such as U-Net [24], and a topology-aware feature synthesis network was proposed to correct the prediction topology based on the Euler characteristic [17]. Proxy tasks were also introduced to help the model focus on the structure topology such as the centerline extraction or distance-map computation [15]. Many works proposed dedicated loss functions to improve the result connectivity [6, 9, 11, 19, 26, 27, 32]. All these connectivity-preserving strategies assume that a large annotated dataset is available, which is rarely the case in vascular imaging applications.

Another research direction was explored consisting in the design of post-processing techniques dedicated to the reconnection of vascular segmentations results. Various algorithms have been suggested, relying on centerlines [7], graphs [12, 23], and contour completion processes [37]. These approaches are complex to use due to their high dependence on parameter selection, and none of them provide the code necessary to reproduce or compare their results.

In our previous work [2], we proposed a strategy to train the reconnecting model and used it to develop an unsupervised plug-and-play segmentation approach. We recognized the potential for the reconnecting term to be applied more broadly as a post-processing step for any type of vascular segmentation result. In the present article, we thoroughly investigate this idea. In particular, we

analyse the properties of the reconnecting term, including the influence of the disconnection size parameter, and its convergence. Additionally, we demonstrate the usefulness and versatility of this novel post-processing strategy by applying it to outputs from various segmentation approaches and datasets.

## 2 Proposed method

In our previous work [2], we developed a model,  $G_{\text{reco}}$ , based on a residual U-Net [14], that learns to reconnect disconnected vessel-like structures from a binary segmentation result. This model is trained on pairs of images containing connected and disconnected vessel-like structures (see top of Fig. 1).

We proposed an algorithm capable of generating random and realistic disconnections from any binary vascular structure. This algorithm is described in details in Appendix B. We demonstrated that our reconnecting term can be learned either based on manual annotations from the dataset of interest, or solely from synthetic images. This bypasses the need for an annotated dataset while still yielding satisfying results. To control the reconnection power of our model, we generated disconnections with sizes drawn from a Gaussian distribution with mean  $s$  and standard deviation  $\sigma$ . In this work, we propose to use this reconnecting model as a post-processing step by applying it iteratively until most disconnections have been filed (see bottom of Fig. 1). The code of our approach is available at <https://github.com/creatis-myriad/plugin-and-play-reco-regularization>.

## 3 Experiments

In this section, we first present the experimental set up used in the following experiments. Next, we analyse the impact of various key elements of the method through an ablation study. Finally, we demonstrate its pertinence on segmentations resulting from different methods.

### 3.1 Experimental set up

To analyse and demonstrate the effectiveness of our method, we tested our framework in both 2D and 3D and used synthetic and real datasets. In 2D, we used the DRIVE [33] dataset composed of 40 retinophotographies and their manual vascular annotations, and the STARE [10] dataset composed of 20 manual annotations of retinophotographies. STARE was used to train our reconnecting model and DRIVE was used as a test dataset to apply  $G_{\text{reco}}$ . We also generated a synthetic dataset composed of 20 synthetic vascular trees with OpenCCO [13] that was also used as a training dataset for  $G_{\text{reco}}$ . In 3D, we used the Bullitt [1] and IXI<sup>3</sup> [35] datasets composed of 33 and 22 brain magnetic resonance angiography (MRA) respectively and their manual vascular annotations. IXI was used to train our reconnecting model while Bullitt was used as a test dataset to apply  $G_{\text{reco}}$ .

Our disconnection algorithm was used on the DRIVE, STARE and IXI to generate disconnected vascular trees with several mean disconnection size of  $s$  ( $s \in \{6, 8, 10, 12\}$ ). We experimentally set the standard deviation  $\sigma = 4$  for DRIVE and STARE and to  $\sigma = 2$  for IXI.

The backbone architecture for  $G_{\text{reco}}$  is a residual U-Net model [14] trained for 1000 epochs in 2D and 3000 epochs in 3D. We used an Adam optimizer with a learning rate of  $10^{-3}$ . We employed a

<sup>3</sup> <https://brain-development.org/ixi-dataset/>

weighted Dice loss function as presented in [2] and a batch size of 4. In 2D, the models were trained with an 80% split for training and 20% for validation, while in 3D, the split was 90% for training and 10% for validation. The final model was selected based on the best validation loss achieved during the training.

There is no single metric that can reflect the quality of vascular segmentations. Depending on the specifics of the clinical questions, different properties of the vascular segmentation may be prioritized. Because we focus on connectivity we chose the three following different metrics: the classic Dice coefficient (DSC) evaluates the global quality of the segmentation, the Average Symmetric Surface Distance (ASSD) evaluates the segmentation without volumetric bias, and the error ratio of the number of connected components  $\epsilon_{\beta_0}$  evaluates the segmentation connectivity. This error ratio is defined as  $\epsilon_{\beta_0} = \left| \frac{\beta_0 - \beta_{0_{\text{gt}}}}{\beta_{0_{\text{gt}}}} \right|$ , with  $\beta_0$  the number of connected components of the segmentation and  $\beta_{0_{\text{gt}}}$  the number of connected component of the annotation. The error ratio was preferred over the value of  $\beta_0$  as  $\beta_0$  is usually larger than 1 in the DRIVE and Bullitt annotations. We finally included the Area Under the Curve (AUC), another metric evaluating the global segmentation quality, for the 2D experiment, as it is a metric traditionally used in DRIVE benchmarks.

### 3.2 Ablation study

**Influence of the size of the disconnections** The training dataset is a key element of our framework as it defines the concept of what should be connected. The main parameter of this training dataset is the mean size of disconnections, denoted as  $s$ , which has been added to the segmentations. The model  $G_{\text{reco}}$  is designed to reconnect these disconnections. Intuitively, the size of the disconnections  $s$  should be tuned to reflect the size of the disconnections present in the segmentations. A small value may not be sufficient to reconnect a vessel with a large gap, while a large value increases the probability of connecting vessels that should not be connected. However, we aim at designing a post-processing that works on a large range of disconnection sizes and so our approach should not be too sensitive to this value. To assess this sensitivity, we trained four different models, denoted  $G_{\text{reco},s=X}$  (with  $X \in \{6, 8, 10, 12\}$ ), on the OpenCCO dataset which have been disconnected with a mean disconnection size  $X$ . We then tested these 4 models on the annotations of the DRIVE dataset that have also been disconnected with increasing values of  $s$  ( $s = 6, s = 8, s = 10$  or  $s = 12$ ). Hence each model will be tested on disconnections sizes it has not been trained for. In this experiment,  $G_{\text{reco}}$  has only been applied once to the segmentation results. The results are presented in Table 1.

Overall, all models perform well and there is no significant drop in metrics when applied to data exhibiting disconnection sizes significantly different from those in the training dataset. As expected, the Dice coefficient do not show a significant improvement after applying our post-processing as the reconnection fragments only represent a small portion of the overall vessels. However,  $\epsilon_{\beta_0}$  and the ASSD significantly decreases, indicating that our post-processing successfully reconnected fragments of vessels. We also observe that the size of the disconnections in the training dataset seems to correlate well with the reconnections that occur. As expected, models trained on larger disconnections tend to perform better on large disconnections (see Appendix A), while still facing challenges in reconnecting smaller disconnections. The model trained with disconnections with a size of  $s = 8$ , seems a good compromise between efficacy in reconnecting and avoiding excessive false connections.

In this experiment, we chose to evaluate our models after applying them only once, to better understand their behavior. However, our goal is to use  $G_{\text{reco}}$  iteratively to reconnect disconnections

Training \ Test	$s = 6$			$s = 8$			$s = 10$			$s = 12$		
	DSC $\uparrow$	ASSD $\downarrow$	$\epsilon_{\beta_0}$ $\downarrow$	DSC $\uparrow$	ASSD $\downarrow$	$\epsilon_{\beta_0}$ $\downarrow$	DSC $\uparrow$	ASSD $\downarrow$	$\epsilon_{\beta_0}$ $\downarrow$	DSC $\uparrow$	ASSD $\downarrow$	$\epsilon_{\beta_0}$ $\downarrow$
Before $G_{\text{reco}}$	0.979	0.202	96.811	0.974	0.22	107.367	0.97	0.232	122.198	0.963	0.243	132.617
	$\pm 0.004$	$\pm 0.06$	$\pm 67.065$	$\pm 0.004$	$\pm 0.071$	$\pm 71.883$	$\pm 0.005$	$\pm 0.057$	$\pm 83.665$	$\pm 0.007$	$\pm 0.054$	$\pm 86.553$
$G_{\text{reco},s=6}$	0.983	0.074	<b>11.429</b>	0.98	0.085	<b>14.095</b>	0.978	0.101	<b>15.485</b>	0.974	0.116	<b>17.619</b>
	$\pm 0.003$	$\pm 0.012$	$\pm 8.783$	$\pm 0.003$	$\pm 0.015$	$\pm 10.92$	$\pm 0.004$	$\pm 0.019$	$\pm 10.758$	$\pm 0.004$	$\pm 0.022$	$\pm 13.8$
$G_{\text{reco},s=8}$	<b>0.985</b>	<b>0.067</b>	15.461	<b>0.983</b>	<b>0.077</b>	17.301	<b>0.981</b>	<b>0.09</b>	19.365	<b>0.977</b>	<b>0.103</b>	23.039
	$\pm 0.002$	$\pm 0.013$	$\pm 11.256$	$\pm 0.003$	$\pm 0.014$	$\pm 12.69$	$\pm 0.004$	$\pm 0.019$	$\pm 14.269$	$\pm 0.004$	$\pm 0.02$	$\pm 18.927$
$G_{\text{reco},s=10}$	0.984	0.078	14.61	0.981	0.089	16.829	0.979	0.101	18.82	0.975	0.117	22.056
	$\pm 0.003$	$\pm 0.015$	$\pm 11.223$	$\pm 0.003$	$\pm 0.016$	$\pm 13.051$	$\pm 0.004$	$\pm 0.023$	$\pm 14.516$	$\pm 0.004$	$\pm 0.017$	$\pm 17.864$
$G_{\text{reco},s=12}$	0.982	0.089	16.232	0.98	0.102	18.561	0.977	0.118	19.776	0.974	0.126	20.612
	$\pm 0.003$	$\pm 0.015$	$\pm 12.213$	$\pm 0.003$	$\pm 0.017$	$\pm 13.75$	$\pm 0.004$	$\pm 0.024$	$\pm 14.034$	$\pm 0.004$	$\pm 0.019$	$\pm 16.189$

Table 1: Quantitative results of applying  $G_{\text{reco}}$  trained on the OpenCCO dataset with several values of  $s$  and applied on the Drive dataset with several values of  $s$ .

that could not necessarily be addressed in a single iteration. We analysed the interest of this iterative approach and evaluate its convergence in the next experiment.

**Convergence of the proposed approach** We propose to apply  $G_{\text{reco}}$  iteratively to reconnect vessels gradually instead of attempting to reconnect across a long range all at once. Our intuition suggests that this approach should limit the creation of false reconnections. In this experiment, we aim first at validating this hypothesis. Secondly, considering the limited number of disconnections in an image, we anticipate that applying  $G_{\text{reco}}$  iteratively will converge to a fixed-point image where all disconnections are filled. In this section we thus explore the experimental convergence of our framework.

We used the same 4 reconnection models  $G_{\text{reco},s=X}$  ( $X \in \{6, 8, 10, 12\}$ ) and applied each one on the Drive dataset which have been disconnected with several mean disconnection sizes ( $s \in \{6, 8, 10, 12\}$ ). The results are presented in Figure 2.

We observe that applying  $G_{\text{reco}}$  iteratively converges as shown by Figure 2(a). Interestingly this convergence occurs even though  $G_{\text{reco}}$  was applied to images with disconnection sizes different from those it was trained on. This highlights the robustness of our approach.

Figures 2 (b-d) show that the size of the disconnections in the training dataset have an impact on the quality of the reconnections made on the segmentation results. The model trained on the dataset created with the parameter  $s = 8$  appeared to be a good compromise between significant reconnections (small  $\epsilon_{\beta_0}$ ) and limiting false reconnections (small ASSD and high DSC values). Moreover applying iteratively  $G_{\text{reco}}$  on the segmentations improve the connectivity of the vascular network and converges to a fixed-point image, regardless of the trained disconnections sizes. Qualitative results are discussed in Appendix A.

Applying our method on artificially disconnected images let us analyse precisely the behavior of our reconnecting term but this introduced a bias since we used the same algorithm to generate disconnections in both the training and test datasets. The next section will explore the behavior of our reconnecting approach in a more realistic scenario.

### 3.3 Applications

In this experiment, we applied our post-processing to real 2D and 3D segmentation results obtained from both an unsupervised variational approach and a supervised deep learning approach.

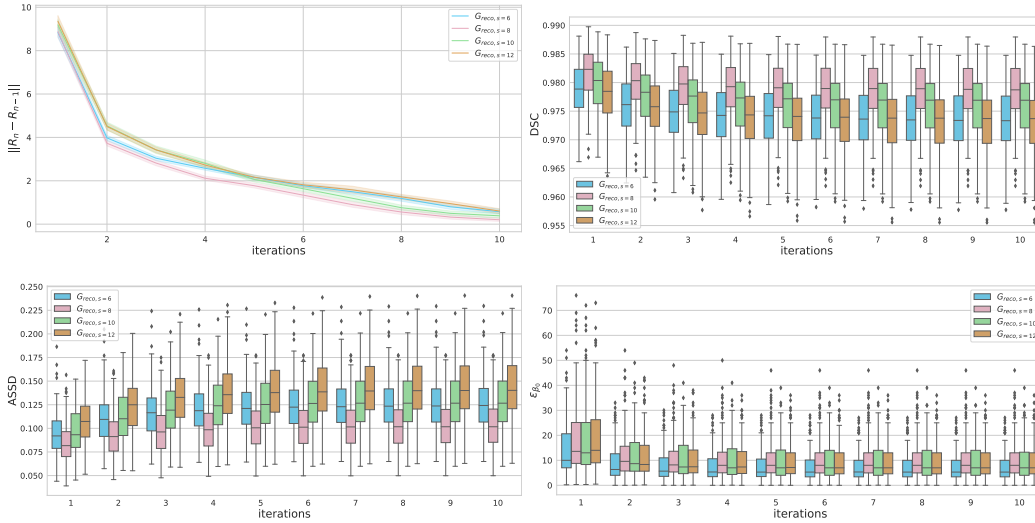


Fig. 2: Results of applying  $G_{\text{reco}}$ , trained on OpenCCO, on the DRIVE annotations artificially disconnected with sizes  $s \in \{6, 8, 10, 12\}$ . (a) convergence curves displaying the  $\ell_2$  norm of the difference of the last two consecutive results. (b-d) quantitative results of our models applied with an increasing number of iterations.

Specifically, we used the variational segmentation method proposed by Chan *et al.* [4] with a total variation [28] regularization. A state-of-the-art U-Net architecture was used as the supervised approach as detailed in [2]. The variational segmentation yields disconnected and noisy results whereas the supervised one produces more complete and connected segmentations. We chose to evaluate our framework on these two different types of results to highlight the versatility of our post-processing method. We conducted experiments both on 2D and 3D images. In 2D, we trained our reconnecting model  $G_{\text{reco}}$  either on the synthetic OpenCCO dataset, denoted as  $G_{\text{reco},CCO}$ , or the STARE dataset, denoted as  $G_{\text{reco},STARE}$ , that have both been disconnected with a mean disconnection size set to  $s = 8$ . We ran both segmentation strategies (variational and deep-learning) on the DRIVE dataset and applied our post-processing.

In 3D, we trained our reconnecting model on the IXI dataset, denoted as  $G_{\text{reco},IXI}$ , that have been disconnected with a mean disconnection size set to  $s = 8$ . We ran both segmentation strategies on the Bullitt dataset and applied our post-processing. Results are summarized in Table 2, Figure 3 and in Appendix A.

We observe that, in general, our post-processing either slightly increases the DSC and ASSD values of the segmentations or does not significantly change them (p-value  $< 0.05$ ). The slight decrease in the ASSD of the 3D variational approach and the DSC of the 3D deep learning approach can be attributed to some false reconnection of aligned artifacts. The overall stability of the DSC and ASSD metrics is expected, because our post-processing primarily involves adding a few pixels to reconnect vessels. These additional pixels represent only a small fraction of the total number of true positive pixels in the image, thus minimally impacting the DSC or ASSD. By contrast, we anticipate a drastic decrease in the connectivity metric  $\epsilon_{\beta_0}$ , since our post-processing affects the connectivity of the segmentations. This is indeed observed. Specifically, we note a decrease of  $> 90\%$

Training \ Test		Variational approach				Deep Learning			
		DSC	ASSD	$\epsilon_{\beta_0}$	AUC	DSC	ASSD	$\epsilon_{\beta_0}$	AUC
2D	Segmentation	0.758 $\pm 0.025$	<b>2.017</b> $\pm 0.452$	98.54 $\pm 91.88$	0.838 $\pm 0.025$	<b>0.811</b> $\pm 0.015$	<b>1.155</b> $\pm 0.181$	34.04 $\pm 26.86$	0.901 $\pm 0.023$
	$G_{\text{recoCCO}}$	0.767 $\pm 0.023$	2.423 $\pm 0.582$	9.003 $\pm 11.39$	0.850 $\pm 0.025$	0.809 $\pm 0.016$	1.192 $\pm 0.19$	<b>9.111</b> $\pm 7.606$	<b>0.903</b> $\pm 0.022$
	$G_{\text{recoSTARE}}$	<b>0.768</b> $\pm 0.023$	2.332 $\pm 0.533$	<b>6.609</b> $\pm 5.817$	<b>0.851</b> $\pm 0.025$	0.810 $\pm 0.015$	1.198 $\pm 0.183$	11.37 $\pm 9.095$	<b>0.903</b> $\pm 0.022$
	p-values	$\sim 10^{-6}$	0.057	$\sim 10^{-6}$	$\sim 10^{-6}$	0.832	0.466	$\sim 10^{-6}$	0.811
3D	Segmentation	0.476 $\pm 0.02$	<b>3.587</b> $\pm 0.42$	26.56 $\pm 10.26$	-	<b>0.756</b> $\pm 0.015$	<b>1.488</b> $\pm 0.211$	3.203 $\pm 1.689$	-
	$G_{\text{recoIXI}}$	<b>0.495</b> $\pm 0.019$	4.154 $\pm 0.427$	<b>5.618</b> $\pm 2.411$	-	0.740 $\pm 0.014$	1.552 $\pm 0.21$	<b>1.697</b> $\pm 1.029$	-
	p-values	$\sim 10^{-4}$	$\sim 10^{-6}$	$\sim 10^{-17}$	-	$\sim 10^{-5}$	0.226	$\sim 10^{-10}$	-

Table 2: Quantitative results obtained with our 2D and 3D reconnecting models on variational and deep learning segmentations. The p-values (from the t-test for normal distributions, or Wilcoxon test otherwise) are shown between the segmentation and  $G_{\text{recoSTARE}}$  in 2D and the segmentation and  $G_{\text{recoIXI}}$  in 3D.

in 2D, and  $> 80\%$  in 3D for the variational approach, and  $> 67\%$  in 2D, and  $> 47\%$  in 3D for the deep learning approach.

It is interesting to note that the model trained on the synthetic OpenCCO dataset yields slightly less inferior results, often due to the creation of false connections. Our reconnecting terms learns to reconnect only based on geometric features. Therefore, the closer the geometry of the vessels in the training dataset to that of the test dataset, the better the performance tends to be. Nonetheless, the drop of performance is quite small which makes our term very useful in a purely unsupervised context in 2D when no vascular annotation is available. In 3D, to the best of our knowledge, there is no synthetic vascular network generation software that yields vascular trees geometrically close enough to a real brain vascular network. In particular, the tortuosities of brain vascular network is much higher than what is possible to generate with softwares like VascuSynth<sup>4</sup> or OpenCCO.

## 4 Conclusion

In this article, we introduced a novel vascular segmentation post-processing to favor vascular network connectivity. This post-processing can be used in an unsupervised or supervised context depending on the availability of vascular annotations on the dataset of interest. We conducted an extensive validation of our approach both in 2D and 3D and showed that our post-processing is robust to the size of disconnections, converges to a reconnected result when used iteratively and significantly improve the connectivity of segmentation results. This approach is purely based on geometric properties of the vessels in binary segmentations and thus some false reconnections may appear. Future work include taking into account the intensities of the underlying image to avoid these false reconnections.

<sup>4</sup> <https://vascusynth.cs.sfu.ca/Welcome.html>

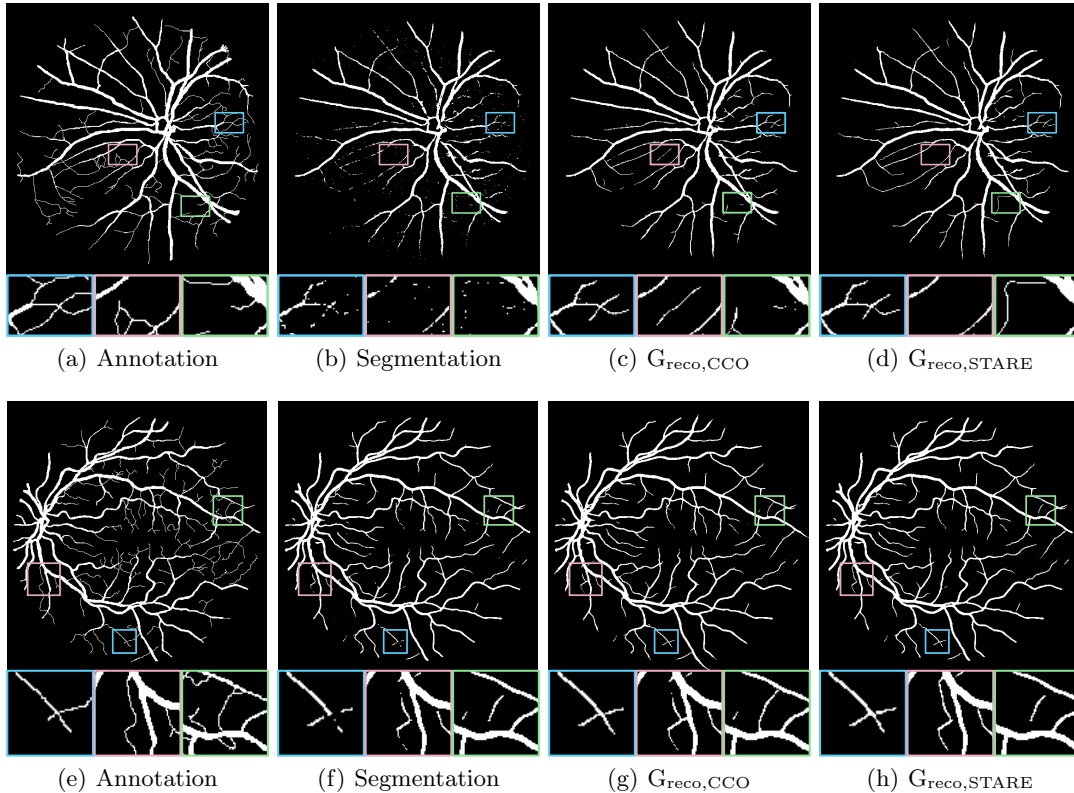


Fig. 3: Results of our post-processing applied to a DRIVE segmentation result from the variational (top row) and deep learning approach (bottom row). (b) and (f) depict segmentation results from variational and deep learning approaches respectively, before post-processing with  $G_{\text{reco}}$ .  $G_{\text{reco}}$  is trained on either the synthetic OpenCCO dataset (c) and (g) or the real STARE dataset (d) and (h).

## 5 Acknowledgments

This work was supported by Agence Nationale de la Recherche (ANR-22-CE45-0018, ANR-18-CE45-0018), LABEX PRIMES (ANR-11-LABX-0063). This work was granted access to the HPC resources of IDRIS under the allocations 2022-AD011013887 and 2023-AD011014452 made by GENCI.

## References

1. E. Bullitt et al. Vessel tortuosity and brain tumor malignancy: A blinded study. *Academic Radiology*, 2005.
2. S. Carneiro Esteves, A. Vacavant, and O. Merveille. A plug and play framework for curvilinear structures segmentation based on a learned reconnecting regularization. *Available at SSRN 4573124*.
3. J. F. Carrillo, M. H. Hoyos, E. E. Dávila, and M. Orkisz. Recursive tracking of vascular tree axes in 3d medical images. *International Journal of Computer Assisted Radiology and Surgery*, 1:331–339, 2007.



4. T. Chan, S. Esedoglu, and M. Nikolova. Algorithms for finding global minimizers of image segmentation and denoising models. *SIAM journal on applied mathematics*, 66(5):1632–1648, 2006.
5. M. Chung, J. Lee, J. W. Chung, and Y.-G. Shin. Accurate liver vessel segmentation via active contour model with dense vessel candidates. *Computer methods and programs in biomedicine*, 166:61–75, 2018.
6. J. R. Clough, N. Byrne, I. Oksuz, V. A. Zimmer, J. A. Schnabel, and A. P. King. A topological loss function for deep-learning based image segmentation using persistent homology. *IEEE transactions on pattern analysis and machine intelligence*, 44(12):8766–8778, 2020.
7. H. Du, X. Zhang, G. Song, F. Bao, Y. Zhang, W. Wu, and P. Liu. Retinal blood vessel segmentation by using the ms-lsdnet network and geometric skeleton reconnection method. *Computers in Biology and Medicine*, 153:106416, 2023.
8. A. F. Frangi, W. J. Niessen, K. L. Vincken, and M. A. Viergever. Multiscale vessel enhancement filtering. In *Medical Image Computing and Computer-Assisted Intervention—MICCAI’98: First International Conference Cambridge, MA, USA, October 11–13, 1998 Proceedings 1*, pages 130–137. Springer, 1998.
9. L. Hakim, M. S. Kavitha, N. Yudistira, and T. Kurita. Regularizer based on euler characteristic for retinal blood vessel segmentation. *Pattern Recognition Letters*, 149:83–90, 2021.
10. A. Hoover, V. Kouznetsova, and M. Goldbaum. Locating blood vessels in retinal images by piecewise threshold probing of a matched filter response. *IEEE Transactions on Medical imaging*, 19(3):203–210, 2000.
11. X. Hu, F. Li, D. Samaras, and C. Chen. Topology-preserving deep image segmentation. *Advances in neural information processing systems*, 32, 2019.
12. V. S. Joshi, M. K. Garvin, J. M. Reinhardt, and M. D. Abramoff. Identification and reconnection of interrupted vessels in retinal vessel segmentation. In *2011 IEEE International Symposium on Biomedical Imaging: From Nano to Macro*, pages 1416–1420. IEEE, 2011.
13. B. Kerautret, P. Ngo, N. Passat, H. Talbot, and C. Jaquet. OpenCCO: An Implementation of Constrained Constructive Optimization for Generating 2D and 3D Vascular Trees. *Image Processing On Line*, 13:258–279, 2023. <https://doi.org/10.5201/ipol.2023.477>.
14. E. Kerfoot, J. Clough, I. Oksuz, J. Lee, A. King, and J. Schnabel. Left-ventricle quantification using residual u-net. In *International Workshop on Statistical Atlases and Computational Models of the Heart*, pages 371–380, 2018.
15. D. Keshwani, Y. Kitamura, S. Ihara, S. Iizuka, and E. Simo-Serra. Topnet: Topology preserving metric learning for vessel tree reconstruction and labelling. In *Medical Image Computing and Computer Assisted Intervention—MICCAI 2020: 23rd International Conference, Lima, Peru, October 4–8, 2020, Proceedings, Part VI 23*, pages 14–23. Springer, 2020.
16. J. Lamy, O. Merveille, B. Kerautret, and N. Passat. A benchmark framework for multi-region analysis of vesselness filters. *IEEE Transactions on Medical Imaging*, PP:1–1, 07 2022.
17. L. Li, Q. Ma, C. Ouyang, Z. Li, Q. Meng, W. Zhang, M. Qiao, V. Kyriakopoulou, J. V. Hajnal, D. Rueckert, et al. Robust segmentation via topology violation detection and feature synthesis. In *International Conference on Medical Image Computing and Computer-Assisted Intervention*, pages 67–77. Springer, 2023.
18. W. Liao, S. Wörz, C.-K. Kang, Z.-H. Cho, and K. Rohr. Progressive minimal path method for segmentation of 2d and 3d line structures. *IEEE transactions on pattern analysis and machine intelligence*, 40(3):696–709, 2017.
19. M. Lin, K. Zepf, A. N. Christensen, Z. Bashir, M. B. S. Svendsen, M. Tolsgaard, and A. Feragen. Dtunet: Learning topological similarity for curvilinear structure segmentation. In *International Conference on Information Processing in Medical Imaging*, pages 654–666. Springer, 2023.
20. O. Merveille, B. Naegel, H. Talbot, and N. Passat.  $n$  d variational restoration of curvilinear structures with prior-based directional regularization. *IEEE Transactions on Image Processing*, 28(8):3848–3859, 2019.
21. O. Merveille, H. Talbot, L. Najman, and N. Passat. Curvilinear structure analysis by ranking the orientation responses of path operators. *IEEE Transactions on Pattern Analysis and Machine Intelligence (PAMI)*, 40(2):304–317, 2018.

22. O. Miraucourt, A. Jezierska, H. Talbot, S. Salmon, and N. Passat. Variational method combined with frangi vesselness for tubular object segmentation. In *Computational & Mathematical Biomedical Engineering (CMBE)*, pages 485–488, 2015.
23. L. Mou, L. Chen, J. Cheng, Z. Gu, Y. Zhao, and J. Liu. Dense dilated network with probability regularized walk for vessel detection. *IEEE Transactions on Medical Imaging*, 39(5):1392–1403, 2020.
24. L. Mou, Y. Zhao, H. Fu, Y. Liu, J. Cheng, Y. Zheng, P. Su, J. Yang, L. Chen, A. F. Frangi, et al. Cs2-net: Deep learning segmentation of curvilinear structures in medical imaging. *Medical image analysis*, 67:101874, 2021.
25. Y. Peng, L. Pan, P. Luan, H. Tu, and X. Li. Curvilinear object segmentation in medical images based on odos filter and deep learning network. *arXiv preprint arXiv:2301.07475*, 2023.
26. Y. Qiu, Z. Li, Y. Wang, P. Dong, D. Wu, X. Yang, Q. Hong, and D. Shen. Corsegrec: a topology-preserving scheme for extracting fully-connected coronary arteries from ct angiography. In *International Conference on Medical Image Computing and Computer-Assisted Intervention*, pages 670–680. Springer, 2023.
27. P. Rougé, N. Passat, and O. Merveille. Cascaded multitask u-net using topological loss for vessel segmentation and centerline extraction, 2023.
28. L. I. Rudin, S. Osher, and E. Fatemi. Nonlinear total variation based noise removal algorithms. *Physica D: nonlinear phenomena*, 60(1-4):259–268, 1992.
29. P. Sanchesa, C. Meyer, V. Vigon, and B. Naegel. Cerebrovascular network segmentation of mra images with deep learning. In *2019 IEEE 16th international symposium on biomedical imaging (ISBI 2019)*, pages 768–771. IEEE, 2019.
30. Y. Sato, S. Nakajima, N. Shiraga, H. Atsumi, S. Yoshida, T. Koller, G. Gerig, and R. Kikinis. Three-dimensional multi-scale line filter for segmentation and visualization of curvilinear structures in medical images. *Medical image analysis*, 2(2):143–168, 1998.
31. T. Shi, N. Boutry, Y. Xu, and T. Géraud. Local intensity order transformation for robust curvilinear object segmentation. *IEEE Transactions on Image Processing*, 31:2557–2569, 2022.
32. S. Shit, J. C. Paetzold, A. Sekuboyina, I. Ezhov, A. Unger, A. Zhylyka, J. P. Pluim, U. Bauer, and B. H. Menze. cldice-a novel topology-preserving loss function for tubular structure segmentation. In *Proceedings of the IEEE/CVF Conference on Computer Vision and Pattern Recognition*, pages 16560–16569, 2021.
33. J. Staal, M. D. Abràmoff, M. Niemeijer, M. A. Viergever, and B. Van Ginneken. Ridge-based vessel segmentation in color images of the retina. *IEEE transactions on medical imaging*, 23(4):501–509, 2004.
34. G. Tetteh, V. Efremov, N. D. Forkert, M. Schneider, J. Kirschke, B. Weber, C. Zimmer, M. Piraud, and B. H. Menze. Deepvesselnet: Vessel segmentation, centerline prediction, and bifurcation detection in 3-d angiographic volumes. *Frontiers in Neuroscience*, page 1285, 2020.
35. N. Valderrama, I. Pitsiorlas, L. Vargas, P. Arbelaez, and M. A. Zuluaga. Job-vs: Joint brain-vessel segmentation in tof-mra images. In *ISBI 2023, IEEE International Symposium on Biomedical Imaging, 18-21 April 2023, Cartagena de Indias, Colombia*, Cartagena de Indias, 2023.
36. A. Vaswani, N. Shazeer, N. Parmar, J. Uszkoreit, L. Jones, A. N. Gomez, L. Kaiser, and I. Polosukhin. Attention is all you need. *Advances in neural information processing systems*, 30, 2017.
37. J. Zhang, E. Bekkers, D. Chen, T. T. Berendschot, J. Schouten, J. P. Pluim, Y. Shi, B. Dashtbozorg, and B. M. ter Haar Romeny. Reconnection of interrupted curvilinear structures via cortically inspired completion for ophthalmologic images. *IEEE Transactions on Biomedical Engineering*, 65(5):1151–1165, 2018.

## A Qualitative results

Figure A.1 compares the results of applying our post-processing model trained with several values of  $s$ , on a Drive image that has been disconnected with a specific disconnection size.

Figure. A.2 shows the evolution of the applying our post-processing several times on a disconnected image from the DRIVE dataset. In the blue and red box of , we can observe that some disconnections that were not successfully reconnected with a single iteration, are gradually reconnected with additional iterations. However, it is worth noting that some false reconnections may still occur, as shown in the green box. Interestingly, these false reconnections often occur when noise fragments are present near a vessel, and  $G_{\text{reco}}$  use them to create realistic vessels.

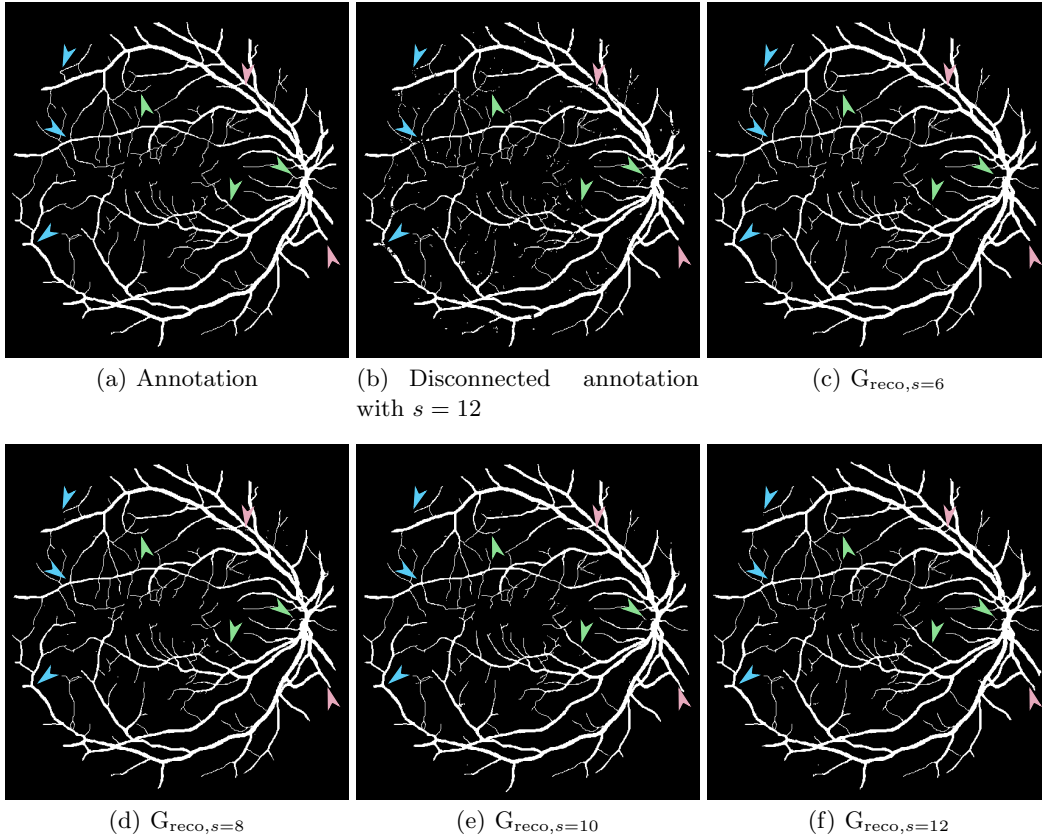


Fig. A.1: Qualitative results of the influence of the disconnection size experiment.  $G_{\text{reco}}$  was trained with a disconnection size  $X$  (with  $X \in \{6, 8, 10, 12\}$ ), denoted  $G_{\text{reco},s=X}$ , on the OpenCCO dataset. A drive dataset annotation (a) was disconnected with  $s = 12$  to obtain (b), followed by a single application of  $G_{\text{reco},s=X}$  on (b), resulting in (c-f). Blue arrows indicate successful reconnections, pink arrows highlight incorrect reconnections, and green arrows denote differences between the results.

Figure A.3 shows the result of our post-processing applied on an image of the Bullitt dataset. The blue arrows point to correct reconnections while the green arrow show a false reconnexion due to noise.

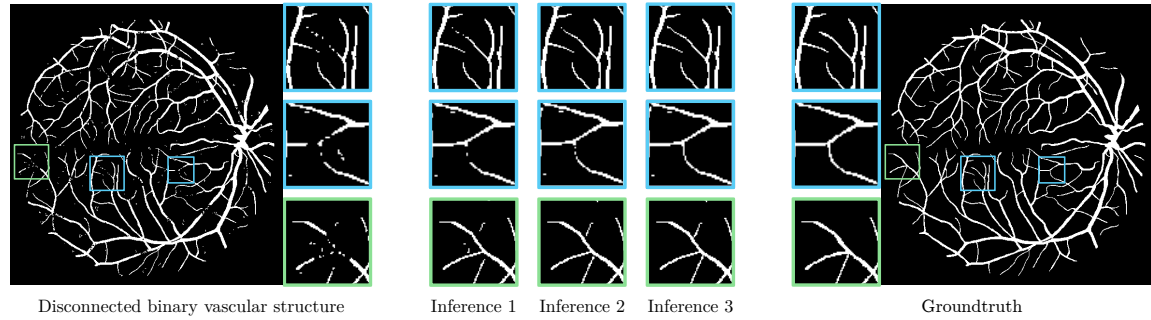


Fig. A.2: Evolution of a DRIVE disconnected manual annotation (with  $s = 12$ ) through successive application of  $G_{\text{reco},s=8}$ .

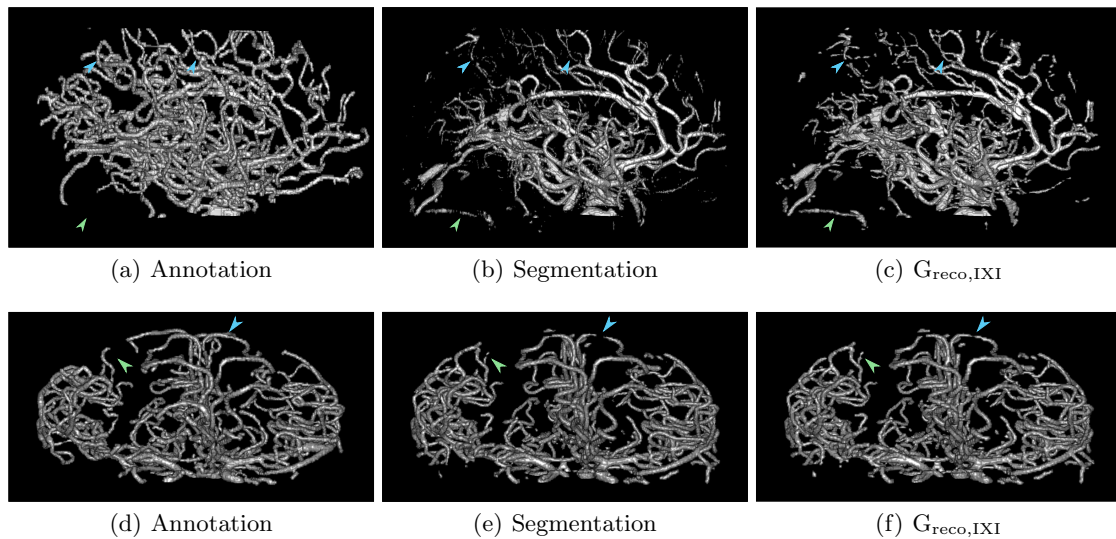


Fig. A.3: Results of our post-processing in 3D. (a) the annotation of a Bullitt dataset image, (b) a segmentation result from a 3D UNet (c) the post-processing result with our reconnecting term trained on the IXI dataset with  $s = 8$ .

## B Disconnection generation algorithm

In this section, we provide a more detailed description of the algorithm we have proposed for generating realistic disconnections in vascular segmentations. The code for this algorithm is available at <https://github.com/creatis-myriad/plugin-and-play-reco-regularization>.

- We compute the segmentation centerline and distance map. The distance map is defined such that each pixel of the segmentation has a value representing the minimum distance to the background. The value of each centerline pixel corresponds to the local radius of the vessel.
- We compute the segmentation centerline and distance map. The distance map is defined such that each pixel of the segmentation has the value of the minimum distance to the background. The value of each centerline pixel correspond to the local radius of the vessel.
- For each disconnection
  - We draw a value  $i \in [1, p]$  from the distribution defined by the probability  $P(i) = \frac{2^{p-i}}{2^p-1}$ , where  $p$  is the maximum radius value in the image. Here  $i$  corresponds to the radius of a vessel in which the disconnection will occur.
  - Randomly select a centerline pixel  $x$  with a radius of  $i$
  - The disconnection size  $d$  is drawn in a Normal distribution  $\mathcal{N}(\frac{s}{i+1}, 0)$ , where  $s$  is the mean disconnection size parameter of our post-processing. The thinner the vessel the longer the disconnection will be.
  - We generate the disconnection by randomly removing  $n$  pixels from the segmentation within a disk of radius  $d$  centered on  $x$ . Here  $n$  is draw from a Normal distribution  $\mathcal{N}(\frac{N}{2}, \frac{N}{4})$  with  $N$  the number of pixels in the disk.
- For each artefact
  - The center  $c$  of the artefact is randomly selected outside of the segmentation mask.
  - A disk of radius  $r$  (where  $r$  is drawn from  $\mathcal{N}(3, 1)$ ) is centered on  $c$ .
  - $n'$  pixels are randomly selected inside the disk and added ( $n' \hookrightarrow \mathcal{N}(\frac{N}{2}, \frac{N}{4})$ ) to the segmentation.